Electrical Power and Energy Systems 158 (2024) 109965

Contents lists available at ScienceDirect

International Journal of Electrical Power and Energy Systems

journal homepage: www.elsevier.com/locate/ijepes

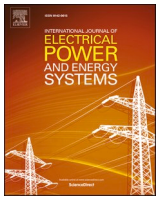

A negative sequence current injection (NSCI)-based active protection scheme for islanded microgrids

Zhenkun Yang *, Adam Dyśko, Agustí Egea-Àlvarez

University of Strathclyde, Department of Electronic and Electrical Engineering, Glasgow G1 1RD, United Kingdom

ARTICLE INFO

Keywords:
Active protection method
Fault direction indicator
High impedance fault
Microgrid
Negative sequence current injection

ABSTRACT

The growing penetration of converter interfaced generation creates unprecedented challenges to protection strategies at all voltage levels. This paper proposes a novel Negative Sequence Current Injection (NSCI)-based active protection scheme for islanded microgrids. The faulty section identification method based on the negative sequence current increment between the pre-injection and current generation steady state conditions enables the scheme to achieve an excellent High Impedance Fault (HIF) detection capability. The proposed NSCI control algorithm maintains the phase angle of the negative sequence current fixed during injection progress, thus providing a highly discriminative feature which facilitates the correct identification of the faulty section. As no form of communication is required the proposed protection scheme can be very cost-effective and flexible in practical applications. Following the detailed description of the principle of operation and the setting procedure, a systematic simulation-based validation is undertaken considering a variety of influencing factors such as fault type, resistance and position, as well as impact of load distribution under HIFs, and possible presence of Synchronous Generators (SGs). The results show that the scheme has an excellent detection and discrimination ability, especially during unbalanced faults, and is not affected by load distribution or behaviour of other sources, including SG.

1. Introduction

With continually increasing proportion of renewables in the power system generation mix, resulting from the internationally accepted zero-carbon emission targets [1], the converter-interfaced Distributed Generation (DG) is playing an increasingly dominant role in the integration of renewable energy sources into existing electricity systems. A microgrid, where the DG is widely applied, is an essential formation of the power system as the penetration of renewables is growing towards 100 % according to some sources [2]. This change has brought many challenges to the existing protection methods.

As this is a known challenge, there are many methods in technical literature which deal with protection issues in microgrids, including both standard approaches and unconventional methods. The authors of [3] and [4] use differential protection in distribution system, which can be effective but typically is quite costly owing to the onerous communication requirements. In [5] and [6], traveling wave-based protection methods are proposed to isolate the faulty section rapidly, however, communication is still a challenge and sampling frequency needs to be carefully selected. A number of papers utilize an adaptive approach where protection adjusts the relay settings according to network topology [7] or fault level [8]. However, these methods usually require full knowledge of the network in advance and/or heavy calculation during operation [9], significantly increasing complexity of such schemes. More recently, artificial intelligence-based protection methods are being proposed to identify the HIF [10], however, a huge amount of data from fault inception tests is required for training purposes, limiting the accessibility in real-life application. As for other methods, a voltage-based scheme is proposed in [11], and a total harmonic distortion-based scheme is suggested in [12], however, these methods might not solve the relay coordination issues.

A separate group of fault detection methods, termed typically as active protection, has also been considered. In this approach the protective device is designed to recognize a specific distinct pattern or a feature in the measured signal which is purposefully generated into the network by an active source. As the inverter connected DGs are highly controllable, they have a great potential to actively participate in the fault detection and clearance process, which may offer notable

* Corresponding author.
E-mail address: zhenkun.yang@strath.ac.uk (Z. Yang).

https://doi.org/10.1016/j.ijepes.2024.109965
Received 15 September 2023; Received in revised form 16 February 2024; Accepted 23 March 2024
Available online 30 March 2024

advantages over the passive approaches. The converter interfaced DG can act both as a current and voltage source and can also rapidly adjust the behavior according to its control algorithm. Often, harmonic, inter-harmonic or sub-harmonic frequencies are generated to distinguish the signal from the fundamental frequency. For example, the authors in [13] configured a differential protection scheme by injecting inter-harmonics. Although interesting idea, it is still expensive for microgrid applications due to communication requirements. In [14], the researcher designed a non-communication scheme using the 5th-order harmonics injection, but the injected signal is only used for fault detection rather than faulty section identification. In [15], all DGs are required to inject different kinds of high-order harmonics to isolate the faulty section, which limits the practical application. In [16], synthetic harmonics are used to protect microgrid, however, communication is still necessary in this method. In [17], a traveling wave based active protection method is built by injecting a current waveform. However, the method is tested only under the network with each measurement point over 30 km away from the injection point, thus it cannot be applied for protecting shorter lines without increasing the bandwidth, and therefore, the cost of hardware.

The work described in this paper can address at least two main challenges: (1) Difficulty in relay coordination when operating in islanded mode. The conventional overcurrent relay assumes that the fault current will flow from a centralized generator to down-stream sections. However, in an islanded microgrid with multiple sources, the relay is likely to suffer from the non-deterministic direction of power flow during faults, leading to protection coordination problems [18]; (2) Cost of protective equipment. The application of advanced protective techniques based on high frequency components or travelling waves can be effective, but due to short line lengths in typical microgrids much higher sampling rates are required to extract the desired fault current features, which incurs higher cost [17].

To address these challenges, this paper proposes a Negative Sequence Current Injection (NSCI)-based active protection scheme capable of identifying and isolating the faulty section in an islanded microgrid. The key novel aspect of the scheme consists in performing active injection of the negative sequence current (from a dedicated inverter connected source) which is combined with negative sequence based faulty line selection. To the authors' best knowledge, even though many negative sequence-based protection methods have been developed [19], all of which are passive methods and there are no published methods which utilize active injection of negative sequence current for protective purposes. With a single active source operating at system frequency (at any location), the scheme enables a simple communication-free time graded design (including backup) which has excellent detection and discrimination capability demonstrated through systematic simulation studies.

The remainder of this paper is organized as follows: Section 2 introduces the operating principle of the proposed scheme. Section 3 describes the optimized process for establishing the protection settings. Section 4 presents the simulation-based performance evaluation and the comparative study of proposed scheme with other methods. Section 5 draws the key conclusions from the paper.

2. Operating principle of NSCI-based scheme

2.1. Protection scheme arrangement and operation

The proposed NSCI-based scheme is designed to operate in islanded mode, which is considered most challenging from the protection standpoint. In grid-connected mode, it is assumed that effective protection scheme can be implemented using more conventional passive methods, and therefore, not considered in this paper.

The scheme requires that the selected buses of the protected microgrid are equipped with the purposefully designed relays which monitor the local voltage and current and can control the circuit breakers of the lines connected to that bus. No communication between the relays is required as all the required signals and data are available locally at each bus or switchboard. This is illustrated using a simplified microgrid with five selected buses presented in Fig. 1 with parameter settings in Table 1. To fulfil the function of a source for active protection, one of the DGs, in this case the Voltage Source Converter (VSC) at bus 3, is equipped with dedicated control feature facilitating negative sequence current injection. To ensure overall stability, the grid-forming functionality for the microgrid is provided by the VSC_1 at bus 1 which is voltage-controlled, and the remaining VSCs at other buses are current-controlled. Each of the VSCs has a rating of 10 MW. The circuit breakers (*CB*s) are installed at the end of each line, and there are also loads (*LD*s) placed at each bus.

The main stages of operation of the NSCI-based protection scheme are illustrated in Fig. 2. Initially, the presence of a fault is detected independently by each relay either by the drop in positive sequence voltage magnitude below 0.95pu, or the increase of negative-to-positive sequence voltage ratio above 0.05pu. The comparison thresholds are selected according to ANSI C84.1 standard [20] in order to detect unbalanced faults, and to provide security against transient load switching of up to 5 MW in a microgrid. Then, it is determined whether the fault is balanced or unbalanced ("Fault type discrimination" in Fig. 2) by comparing the maximum value of local negative sequence current (I_{2max}) against a fixed threshold (I_{2th}) according to (1):

$$I_{2max} > I_{2th} = 0.2I_{2min} = 0.2 \bullet \frac{N_{21} \bullet V_{LL}}{\sqrt{3} \bullet Z_{line,max}} \tag{1}$$

where N_{21} is the minimum value of negative-to-positive sequence voltage ratio when the fault is expected to be detected, i.e., 0.05 pu (refer to fault detection logic in Fig. 2), V_{LL} is nominal line-to-line voltage. The threshold is based on the value of minimum anticipated negative sequence current (I_{2min}) during a solid unbalanced fault, thus the lowest value of I_{2min} (the worst-case scenario) is achieved under the highest possible line impedance in the fault loop ($Z_{line,max}$) in the microgrid. In the test network of Fig. 1, it is the impedance from bus 1 to bus 5. As the total fault loop impedance can be further increased by fault resistance (especially during HIFs), I_{2th} includes additional 80 % sensitivity margin (i.e. threshold set at $0.2I_{2min}$) to ensure high resistive faults can also be detected.

After fault type discrimination, a dedicated DG starts to inject the negative sequence current, which is initiated by the relay connected at the same bus. During the NSCI period the relay at each bus calculates the Fault Direction Indicator (FDI) to identify whether the fault occurred on the Left-Hand-Side (LHS) or Right-Hand-Side (RHS) from the relay. Finally, after considering the tripping logic, the fault is isolated by correct circuit breakers after a pre-set time delay.

Referring to the example in Fig. 1, where a fault occurs on line 4, the presence of the fault is detected by all relays but the relay closest to the active injection DG additionally initiates the NSCI process on the DG controller. In this case REL_3 initiates active injection on VSC_3. This process has two distinct stages: preparatory pre-injection stage, and current generation stage.

During pre-injection stage, the relay at each bus captures the steady state Negative Phase Sequence (NPS) current magnitude and phase angle (evaluated by Fast Fourier Transform). This establishes a reference point for measuring negative sequence current increment during the current generation stage. At the same time, the active DG makes a choice from two different control methods according to fault type discrimination. For balanced faults, angle control is disconnected in the NSCI control algorithm since there is no stable negative sequence current angle. For unbalanced faults, angle control is enabled. The reference for the angle controller is derived from the current which points in the direction of the fault. To select the correct current reference, the Current Angle Selection (CAS) indicator (2) is used, which is defined as the angle difference between one of the negative sequence currents (in this paper the angle of the RHS current θ_{2Rpre} is used) and the bus negative

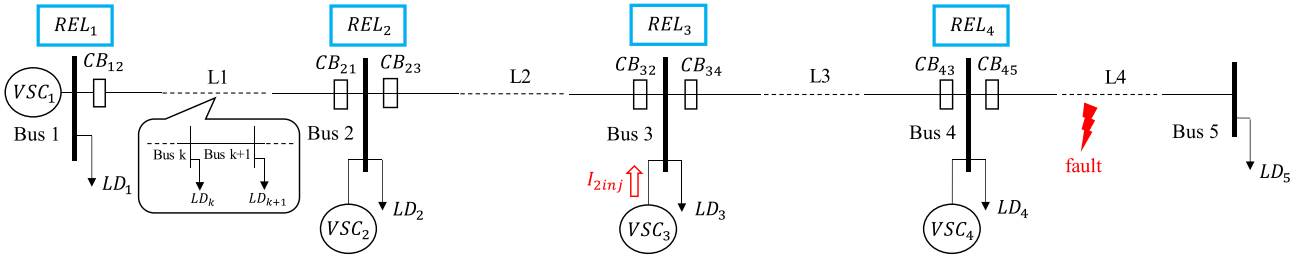

Fig. 1. Microgrid topology.

Table 1
Parameters of the simplified microgrid model.

Simulation parameters	Value
Nominal voltage	11 kV
Nominal frequency	50 Hz
DG rating	10 MVA for each DG
Filter impedance	0.242 + j2.42 Ω for each DG
DG reference power	5 MW for the DG at bus 1, 2&4; 10 MW for the DG at bus 3
Line impedance	0.1 + j0.1 Ω/km for each line
Line length	2.5 km for each line
Load power	5 MW for the load at each selected bus

sequence voltage θ_{2Vpre}.

$$\Delta\theta_{2(CAS)} > |\theta_{2Rpre} - \theta_{2Vpre}| \tag{2}$$

Both angles are measured during the pre-injection stage. The CAS indicator defined in this way, enables correct identification of the fault direction. From the sequence network analysis, it is established that for a fault on the RHS the CAS indicator defined by (2) always has a value above 90°. For any other fault on the LHS, the CAS indicator will be below 90°. The reference angle selection logic is illustrated in the converter controller algorithm in Fig. 5 ('Angle control' at the bottom left corner).

The reference angle ensures that during the current generation stage, injected current flows from the injection bus towards the faulty section and creates the NPS current increment in the microgrid in the same direction as the initial negative sequence fault current. The relay at each bus evaluates the resultant negative sequence current increment between pre-injection stage and current generation stage based on (3). Using this increment, the Fault Direction Indicator (FDI) is determined depending on the type of fault (4). For balanced faults, the magnitude of the current increment is used, while for unbalanced faults, the real part of the increment phasor is utilized.

$$\Delta\mathbf{I}_2 = \mathbf{I}_{2\mathbf{gen}} - \mathbf{I}_{2\mathbf{pre}} = \Delta I_2 \angle \Delta\theta_2 \tag{3}$$

$$\text{FDI} = \begin{cases} \Delta I_2 & \text{(balanced fault)} \\ \Re\{\Delta\mathbf{I}_2\} & \text{(unbalanced fault)} \end{cases} \tag{4}$$

The FDI identifies whether the monitored bus is inside or outside of the Source-to-Fault Path (SFP), i.e., the zone between the injection bus and the fault. Under normal operating condition of the microgrid, only low level of negative sequence current, caused by the unbalanced generation and load, is expected, which is overlapped with the fault current at pre-injection stage. However, this initial unbalance has negligible influence on the proposed method as the protection philosophy is based on the current increment, which is primarily affected by the injected current from active DG.

Fig. 3 shows the two different relay operation modes depending on whether the relay is at a non-injection or an injection bus. For any non-injection bus (Fig. 3(a)), there are at least 2 CBs, one of which is expected to be pointing towards the injection bus while the others pointing away from the injection bus, except for the bus at the end of a radial system (e.g., bus 1 in Fig. 1) where only 1 CB is installed. If the measured point (bus) is determined to be inside SFP (FDI > ΔI_{2th}), the CB pointing away from injection bus will trip but the CB pointing towards the injection bus will be blocked. However, if the bus is determined to be outside SFP (FDI < ΔI_{2th}), the CB facing the injection bus will be activated and the other CB will be blocked. For a relay at an injection bus (Fig. 3(b)), faulty section identification method depends on the result of fault type discrimination. Under balanced fault, if the current measuring point is inside SFP, the CB on the same side as the measuring point will trip; otherwise, the CB on the opposite side will trip. Under unbalanced fault, the fault-side is the same as the side where current angle is selected for NPS current injection, which is determined earlier by CAS indicator (2), therefore, the CB on that side will trip.

To ensure proper faulty section discrimination and to provide backup without the use of communications, all CBs are arranged in a time-graded system. Table 2 shows the time delay settings for the CBs in the microgrid shown in Fig. 1. For the CBs on the LHS of each bus, the time delay increases from bus 2 to bus 4. For the CBs on the RHS of each bus, the time delay increases from bus 4 to bus 1. The relay at bus 1 always trips the RHS CB as there is only one CB. In this way, the relays are coordinated by a time-graded system and the CB with a longer time

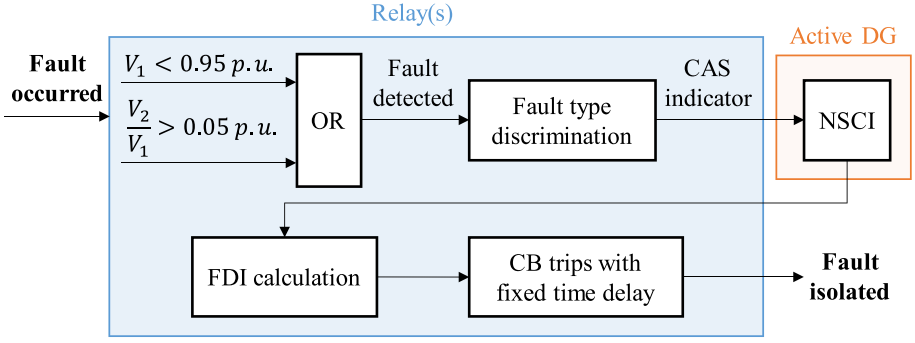

Fig. 2. Fault isolation process.

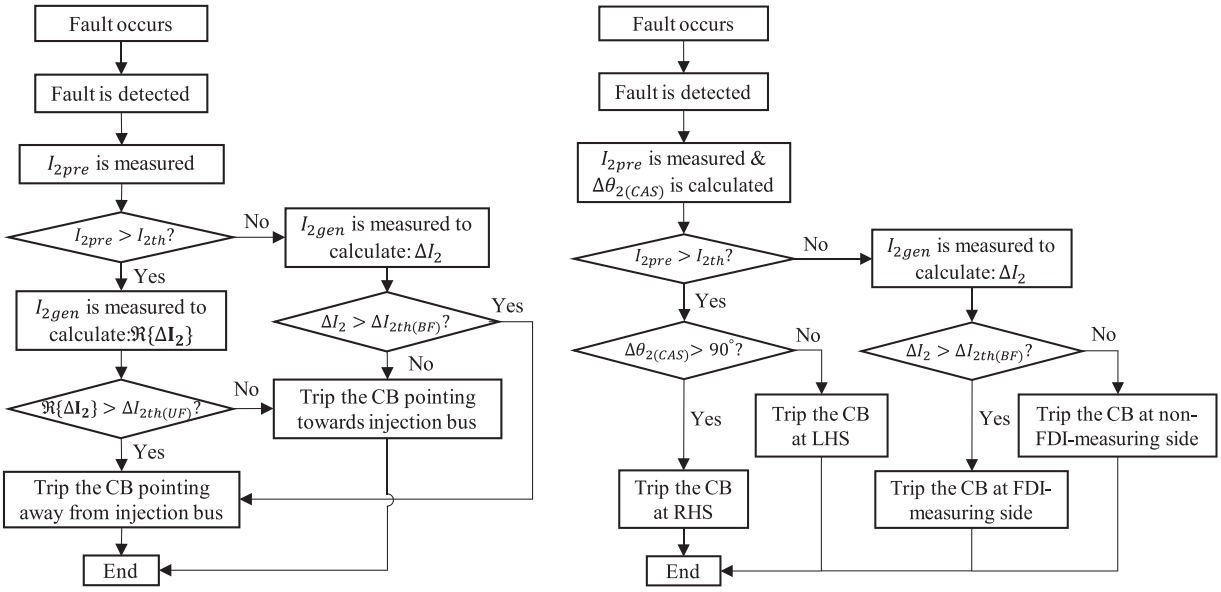

Fig. 3. Relay operation logic following a fault at different buses.

Table 2
Relay time coordination for microgrid in Fig. 1.

Circuit breaker position	Time delay setting (in Seconds)			
	Bus 1	Bus 2	Bus 3	Bus 4
LHS	N/A	0.05	0.2	0.35
RHS	0.5	0.35	0.2	0.05

delay can provide backup for the CB with shorter time delay.

2.2. Negative sequence current injection (NSCI) control

The active current injection is the key element of the proposed scheme. Fig. 4 demonstrates the variation of the positive and negative sequence currents (with their reference values) within the converter of the DG selected for active current injection. Initially, in normal operation, positive sequence current is produced by the converter to generate balanced 3-phase power. When the fault occurs at 0.05 s, the positive sequence current initially increases but as soon as the fault is detected by the relay, the converter ramps down positive sequence current reference to zero. The whole process takes approximately 20 ms. The fault detection time delay around 3 ms results in a small peak during current dynamics before ramping down. The following 40 ms after ramping down is introduced as a waiting time to ensure fault current has reached the steady state, and thus, enabling more accurate measurement of the current phasor (this is pre-injection stage). Then converter injects negative sequence current (generation stage) with trapezoidal magnitude envelope during the following 80 ms, which has the amplitude of 0.3p.u. and this amount of amplitude ensures that the injected current increment can be observed by relay at each selected bus in the microgrid.

Fig. 5 presents the block diagram of the NSCI control algorithm which consists of four main parts: Ramp down current control, trapezoid magnitude control, angle control and Polar to Cartesian transform. Ramp down current control is used to reduce the positive sequence current to zero. Positive sequence current reference is controlled by power control under normal operation, which will be switched to ramp down the current immediately after the fault is detected. The trapezoidal shaping of the magnitude reference signal reduces dynamic oscillations which can otherwise result from step changes in magnitude control. As

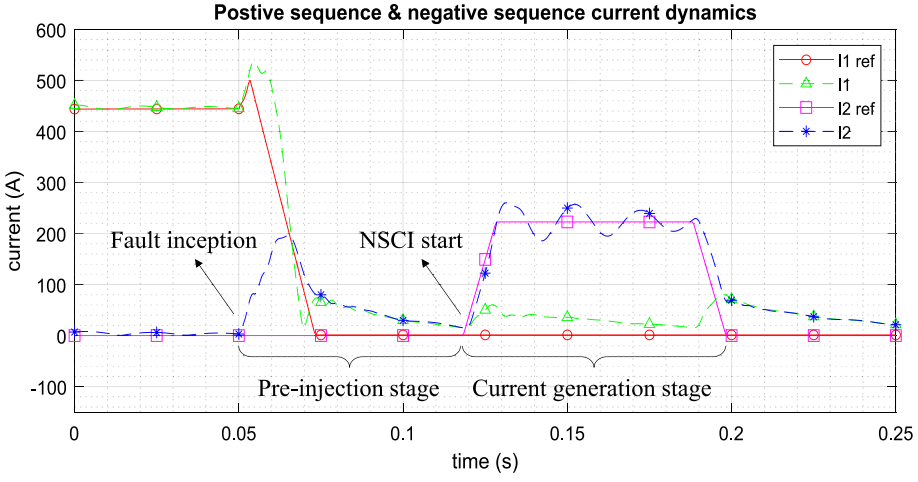

Fig. 4. Current dynamics during NSCI progress.

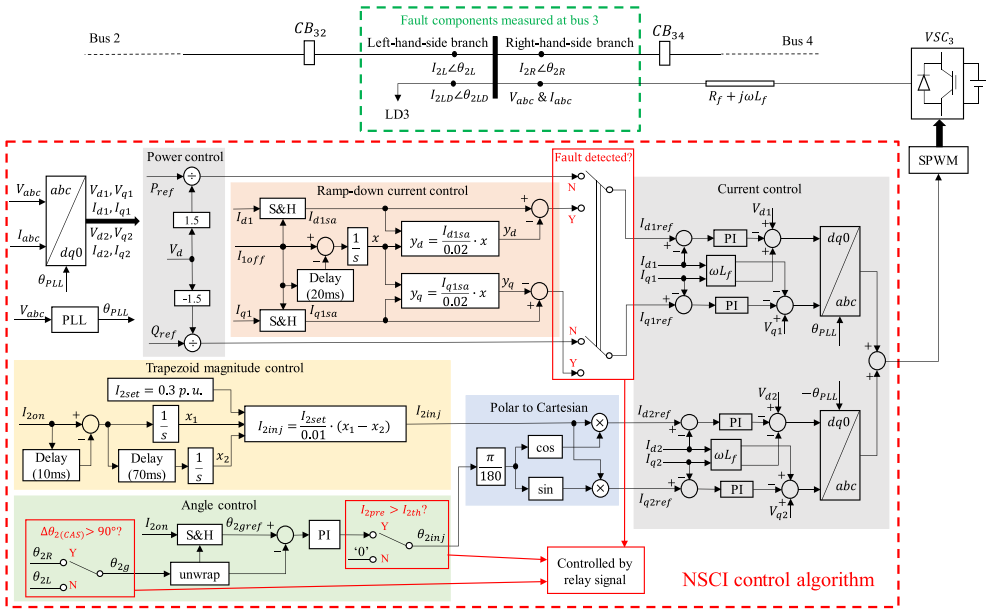

Fig. 5. NSCI control algorithm.

for angle control, the PI controller is disconnected under balanced faults while connected under unbalanced faults to maintain the continuity of the selected current angle during the NSCI injection as defined by (5).

$$\theta_{2inj} = \begin{cases} (\theta_{2gref} - \theta_g)(k_p + k_i/s), & (I_2 > I_{2th}) \\ 0, & (I_2 < I_{2th}) \end{cases} \tag{5}$$

where θ_{2inj} is the injected current angle, θ_{2g} is the selected current angle, θ_{2ref} is the reference value measured from the steady state of θ_{2g} at pre-injection stage. The angle controller has two switches, one switch enables/disables PI angle controller based on the type of fault being detected, and the other switch determines which current phasor angle to take as a reference based on (2). Additionally, to ensure the correct phase angle of the injected NPS current a Polar to Cartesian transformation is used, which will convert the Polar axis components into Cartesian axis components to provide negative sequence current references for converter's inner current control based on (6) and (7):

$$I_{d2ref} = I_{2inj} \bullet cos(\theta_{2inj}) \tag{6}$$

$$I_{q2ref} = I_{2inj} \bullet sin(\theta_{2inj}) \tag{7}$$

For any unbalanced fault, the angle reference is θ_{2gref} which is the angle of the measured NPS current before the injection starts (unwrapped angle of θ_{2g} frozen in memory by the Sample & Hold component, triggered by I_{2on}). For a three-phase balanced fault the angle is set to zero as there is no negative sequence current before the injection starts. The relay operating logic externally controls the position of the logical switches of the DG NSCI controller (indicated by red boxes in Fig. 5). This also includes positive sequence component control which is ramped down to zero after a fault is detected.

3. Evaluation of protection settings

This section explores the current response characteristics during active injection using sequence network analysis, in order to achieve best compromise protection settings for the proposed scheme.

3.1. Current variation characteristic

The measured current at different points in the network is affected by many factors such as the fault type, measuring point location, injected current magnitude and phase, and even the distribution of load impedance. In this paper, the current flow at each measured point during NSCI progress is analyzed using the equivalent circuit as shown in Fig. 6 where $Z_{f(eq)}$ represents the equivalent fault impedance seen from the terminals of the negative sequence network, which under three-phase balanced fault condition is equal to the fault resistance, i.e., $Z_{f(eq)} = R_f$. Under phase-to-phase fault and two-phase to earth fault, $Z_{f(eq)} > R_f$ due to the series connected impedances in positive and negative sequence networks. Under single phase-to-earth fault, $Z_{f(eq)} > 3R_f$, since the positive, negative and zero sequence networks are connected in series together, the current flowing through the measured point is lower due to large $Z_{f(eq)}$.

As an incremental model is used (applying superposition theorem), it is assumed that there are no other sources in the network producing negative sequence current increment at the same time as the active NSCI. Each measured point divides the whole network into two parts with different load impedances. The impedance Z_m is the total equivalent load impedance of the microgrid section which does not include the injection bus, and Z_n is the total equivalent load impedance of the microgrid section which includes the injection bus. The phasor ΔI_2 is the increment between the pre-injection and current generation stages. The solid red line represents the main path where the majority of injected NPS current is flowing from the dedicated DG towards the fault. At the same time, the injected NPS current also flows through the parallel connected impedances of the loads, i.e., Z_m and Z_n, as shown by the dashed red lines. $\Delta I_{2(in)}$ is the current magnitude variation for a

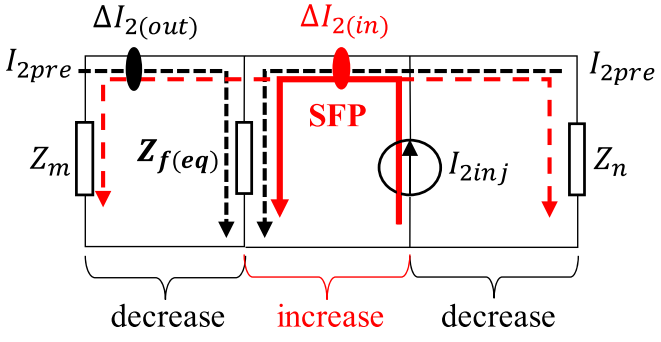

Fig. 6. Equivalent circuit of a microgrid at the current generation stage.

measured point located inside SFP, and $\Delta I_{2(out)}$ is the current magnitude variation for a measured point located outside SFP. At each measured point, the magnitude variation can be approximated using the current divider principle. The conditions of inside and outside SFP are presented in (8) and (9) respectively. Theoretically, with $Z_{f(eq)}$ tending to infinitely, the fault 'disappears' from the circuit and both magnitudes converge to the same value C as defined by (10). As can be seen, the common convergence value C is only related to the injected current magnitude (I_{2inj}) and the load impedance distribution (Z_m and Z_n) in the microgrid.

$$\Delta I_{2(in)} = I_{2inj} \bullet \frac{Z_n}{Z_m \| Z_{f(eq)} + Z_n} \tag{8}$$

$$\Delta I_{2(out)} = I_{2inj} \bullet \frac{Z_n \| Z_{f(eq)}}{Z_m + Z_n \| Z_{f(eq)}} \tag{9}$$

$$\lim_{R_f \to \infty} \Delta I_{2(in)} = \lim_{R_f \to \infty} \Delta I_{2(out)} = I_{2inj} \bullet \frac{Z_n}{Z_m + Z_n} = C \tag{10}$$

Fig. 7(a) and 7(b) demonstrate the relay tripping logic for balanced fault at a specific bus with the threshold $\Delta I_{2th(BF)}$. FDI is always a positive number, and the current increment is equal to the measured current at current generation stage since the negative sequence current at pre-injection stage is zero ($I_{2pre} = 0$). The measured point will be discriminated as inside SFP when $\Delta I_2 > \Delta I_{2th(BF)}$, or outside SFP otherwise. This further determines the tripping of local circuit breakers (LHS or RHS) according to relay operation logic in Fig. 3. Fig. 7(c) and 7(d) show the relay tripping logic for unbalanced fault at a non-injection bus with the threshold $\Delta I_{2th(UF)}$. In this case the real part of the phasor increment is used which can be either positive or negative. The measured point is discriminated as inside SFP if $\Re\{\Delta \mathbf{I}_2\} > \Delta I_{2th(UF)}$ and outside SFP otherwise. The relay operation is determined by the logic shown in Fig. 3 (a). It should be noted that, by design, the DG controller injects the negative sequence current that is aligned in phase with the angle of the measured fault current during the pre-injection stage. Therefore, it is expected that the phase angle of the current increment, i.e., the current angle difference between pre-injection and current generation stages, can only be either close to 0° (measurement inside SFP) or close to 180° (measurement outside SFP). As all phasor increments in the microgrid are expected to be nearly in parallel with the real-axis, it is most appropriate to use the real part of the current increment as a guiding quantity which provides the best directional discrimination.

3.2. Protection setting design

The protection settings under balanced and unbalanced faults need to be looked at differently due to different negative sequence current variation characteristics. To graphically illustrate the adopted protection setting approach, Fig. 8 demonstrates the theoretical variation curve of FDI with respect to fault impedance together with the designed thresholds at one measurement point (bus 2 RHS) in the microgrid in Fig. 1. The curves are charted from the mathematical Eqs. (8), (9) and (10). Under balanced fault, FDI is always positive for the measured points located both inside and outside of SFP. The margin between the conditions of inside and outside SFP is decreasing with the increase of fault impedance since both curves are converging to the common convergence value C. Therefore, the FDI threshold is C as calculated by (10) for each bus. Under unbalanced fault, with the increase of fault impedance, the value of FDI will be positive and converge to 'C' when inside SFP while will be negative and converge to '$-C$' when outside SFP. Therefore, there will always be a large margin between the two conditions to identify the fault direction and the FDI threshold is chosen at $0.2C$.

The choice of $0.2C$ needs further clarification. As the value of C is dependent on load impedance which changes in real time and cannot be accurately pre-determined in most practical cases, the calculation of C is performed under the assumption that the load power is evenly distributed among all buses in the microgrid. However, with the load variation in real life, the actual convergence value can be higher or lower than the one obtained using the assumed load distribution in the microgrid, making HIF protection less effective. To compensate for this simplifying

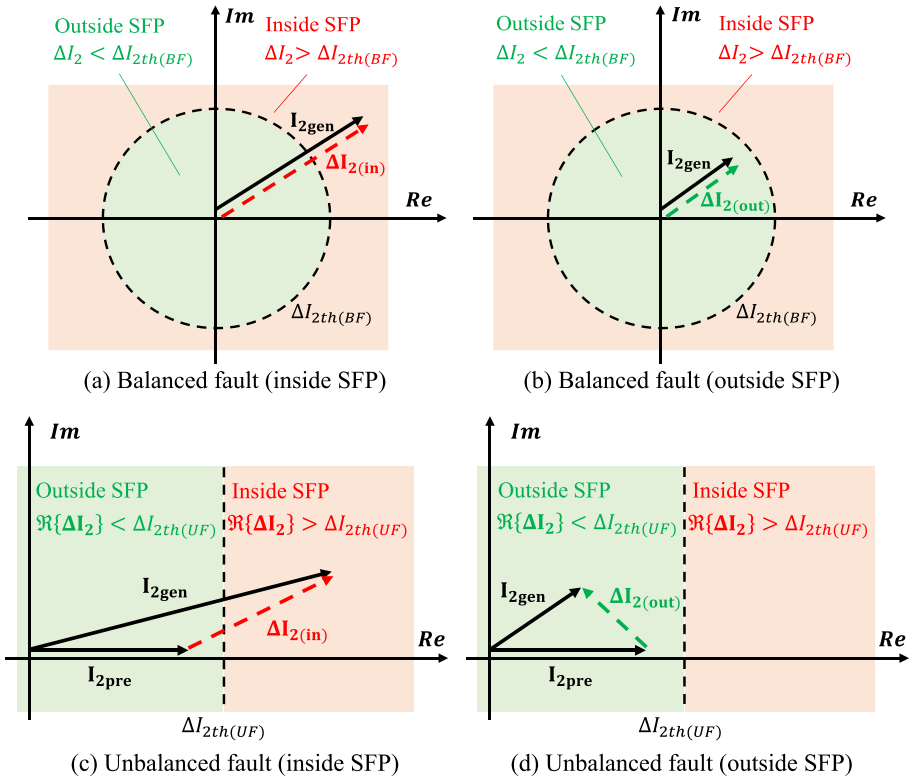

Fig. 7. Relay tripping logic at a specific bus under the conditions of inside and outside SFP for balanced and unbalanced faults.

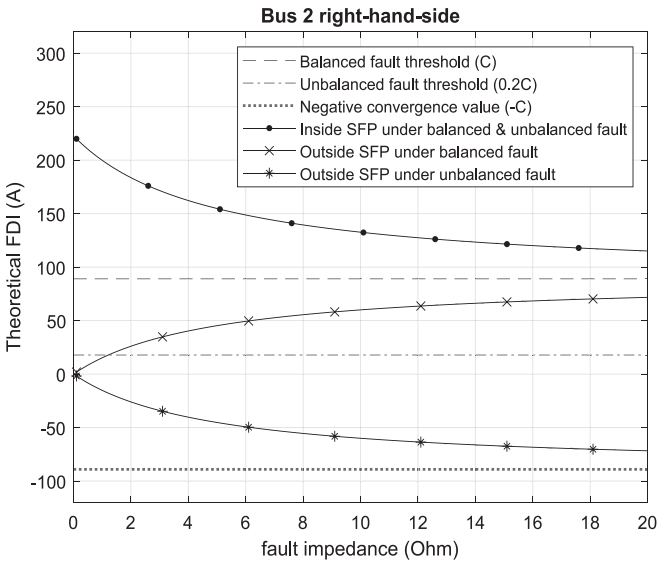

Fig. 8. Theoretical curve and threshold of FDI.

assumption and ensure correct operation under different loading conditions in practice, a sensitivity margin of 80 % is assumed. Setting threshold at $0.2C$ for unbalanced fault can cope with potentially severe load variation which affects the common convergence value. Table 3 summarizes the operations and protection settings under different fault types and buses. For the injection bus the earlier established CAS indicator threshold of 90° is used. The effectiveness of this setting, especially for discrimination under unbalanced faults, will be verified in section 4 through detailed simulation results.

4. Simulation based performance evaluation

The validation test of NSCI-based protection scheme is performed on the islanded microgrid in Fig. 1 with the proposed protection settings applied. Several factors which can influence the scheme response have been considered, including fault type, fault position, fault resistance, and the impact of an additional Synchronous Generator (SG) of varying size. Additionally, to confirm the validity of the assumption about even distribution of loads (made in setting calculation), a few alternative load distributions have been considered both in terms of real power and power factor.

4.1. Assessing the effectiveness of HIF detection

The impact of load distribution on the effectiveness of detecting faults is investigated first, using the test cases 1–5 as defined in Table 4. Case 1 serves as a reference, as it reflects the even load distribution assumed for the calculation of settings (i.e., 5 MVA connected at each bus and operating at unity power factor). To analyze the impact of the demand distribution in the microgrid, the loads nearest to the injection are selected as they are most likely to impact on the protection operation (i.e., loads 3 and 4). The uneven distribution of real power (cases 2 and 3) and power factor (cases 4 and 5) are both included in the test. Under each case a series of fault conditions is considered including different fault types and fault positions in the microgrid. Each simulation is repeated with fault resistance gradually increasing until the scheme stops operating so that the value of maximum detectable fault resistance (R_{fmax}) can be established.

The results for all 5 cases are summarized in Table 5. The highest value around 18.8Ω occurs under balanced fault and the lowest value around 3.8Ω occurs under single phase to earth fault. This is consistent with the sequence network analysis in section 3.1 as the larger equivalent fault impedance in negative sequence circuit is always expected under unbalanced faults which leads to lower fault current, making the fault more difficult to detect. It should be noted that the results confirm that load active and reactive power variation do not have significant influence on the fault detection ability of the scheme. This verifies the assumptions made during the settings calculation relating to load distribution and scheme sensitivity margin. Additionally, it can be observed that in terms of fault location line 1 has the smallest value of R_{fmax} compared to other lines under the same fault type. Since line 1 is nearest to the voltage-controlled VSC_1 (strongest source in the microgrid), the undervoltage based fault detector is somewhat less effective. However, this effect does not have a major impact on the HIF detection ability of the scheme.

Table 3
Summary of operations and protection settings.

Fault type		Balanced fault	Unbalanced fault
Fault type discrimination method		$I_2 < I_{2th}$	$I_2 > I_{2th}$
Injection method		Angle control disconnected	Angle control connected
Non-injection bus	Inside SFP	$\Delta I_2 > C$	$\Re\{\Delta \mathbf{I}_2\} > 0.2C$
	Outside SFP	$\Delta I_2 < C$	$\Re\{\Delta \mathbf{I}_2\} < 0.2C$
Injection bus	Inside SFP	$\Delta I_2 > C$	$\Delta\theta_{2(CAS)} > 90^{\circ}$
	Outside SFP	$\Delta I_2 < C$	$\Delta\theta_{2(CAS)} < 90^{\circ}$

4.2. Performance of the fault direction indicator (FDI)

Assuming the fault has been detected, the correct determination of the fault direction is the second crucial element of the successful fault isolation. This aspect can be particularly challenging during resistive faults. The FDI calculated by each relay during the NPS current generation stage determines the fault direction according to the thresholds presented in Table 3. To better appreciate the impact of various factors on FDI the results in the following subsections are presented graphically. The Figs. 9 to 11 present values of FDI against the setting thresholds (dashed lines) with fault resistance increasing in 1Ω steps. The last point is plotted at the value of R_{fmax} as determined in Table 5.

4.2.1. Impact of fault type and position

The impact of fault type and faulty section on FDI is evaluated at a specific measured position, i.e, bus 4 LHS, which is presented in Fig. 9. It can be seen that under various test conditions, the maximum detected fault resistance R_{fmax} is different, which is determined by the utilized fault detection method (Fig. 2).

Table 4
Load power setting of different test cases.

Case n. o.	Load					
	Load 3		Load 4		Load 1, 2 & 5	
	S (MVA)	Power factor	S (MVA)	Power factor	S (MVA)	Power factor
1	5	1	5	1	5	1
2	9	1	1	1	5	1
3	1	1	9	1	5	1
4	5	0.6	5	1	5	1
5	5	1	5	0.6	5	1

Table 5
Maximum detectable fault resistance (in Ω).

Case n.o.	Fault type & section															
	Balanced fault				Phase B to earth fault				Phase B & C to earth fault				Phase B to C fault			
	Line 1	Line 2	Line 3	Line 4	Line 1	Line 2	Line 3	Line 4	Line 1	Line 2	Line 3	Line 4	Line 1	Line 2	Line 3	Line 4
1	13.1	15.5	17.2	16.7	3.9	5.9	6.6	6.2	8.0	8.9	10.2	9.8	9.0	11.9	13.1	12.4
2	13.4	15.6	17.4	17.0	3.9	5.9	6.7	6.3	8.1	9.3	10.4	10.0	9.0	11.9	13.2	12.6
3	12.8	15.3	17.0	16.3	3.9	5.9	6.6	6.0	7.8	9.1	10.1	9.6	9.0	11.9	13.0	12.2
4	12.6	16.9	18.8	18.2	3.8	5.7	6.5	6.0	8.1	10.2	11.5	10.9	8.9	11.8	13.0	12.3
5	12.6	16.8	18.5	17.8	3.8	5.7	6.5	6.0	8.1	10.1	11.1	10.6	9.0	11.9	13.0	12.3

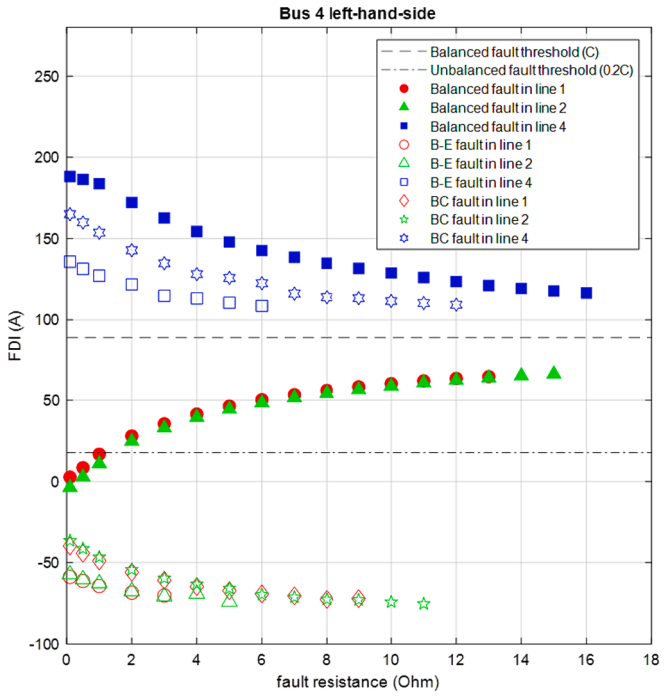

Fig. 9. Impact of fault type & faulty section on FDI (Case 1 condition).

The discrimination margin is the difference between the FDI values for inside SFP and outside SFP measurements. The wider the margin the more effective and reliable the threshold-based discrimination can be. In Fig. 9 it can be seen that under balanced faults, the discrimination margin is getting narrower, as the FDI values are converging towards the value of C as fault resistance increases. This is both for inside SFP measurement (fault on line 4), and outside SFP (i.e., fault on line 1 or 2). Under unbalanced faults, when measured point is inside SFP (fault on line 4), the FDI values are lower compared to balanced fault condition due to the larger $Z_{f(eq)}$ as shown in Fig. 6, but still remain above the value of C. However, when measured point is outside SFP (fault in line 1, 2) the FDI is negative and tends towards $-C$ which preserved great discrimination margin regardless of the fault resistance. Therefore, fault direction can be identified by FDI correctly under all fault conditions and with resistances up to the HIF sensitivity margin. It should be noted that unbalanced faults always have wider discrimination margin.

4.2.2. Impact of load distribution and power factor

Compared with the fault event which does not impact the property (the C) of a microgrid under normal condition, the load power swing has a significant influence on the value of C due to the modification of load impedance distribution in microgrid. The impact of load active power and power factor on the FDI is assessed using the 5 cases as defined in Table 4. In all scenarios the fault is applied in line 3. The FDIs of measured points located at bus 3 RHS (inside SFP) and bus 4 LHS (outside SFP) are used for analysis. The results are presented in Fig. 10 which is divided into part (a) balanced faults, and (b) unbalanced faults.

Under balanced faults, as can be seen from Fig. 10(a), the identification of fault direction can be challenging especially with fault resistance above 10Ω. For example, in Case 2, the FDI at bus 3 RHS reaches the threshold C at $R_f = 17\Omega$, leaving no margin for direction discrimination. Similarly, in Case 3, the FDI at bus 4 LHS reaches the threshold at $R_f \approx 13\,\Omega$. This issue is the direct effect of uneven active power distribution which has a in impact on the convergence value C (due to changing load resistance distribution).

Under unbalanced faults, as in Fig. 10(b), although the FDI at bus 3 RHS (inside SFP) is affected by the load distribution in a similar manner to the balanced fault, the FDI values do not come close the threshold which is now set to $0.2C$. This setting is possible because the FDI at bus 4 LHS (outside SFP) is always negative. Therefore, it can be concluded that under all unbalanced faults, the fault direction identification is not influenced by active power variation at all due to the intrinsically large FDI margin. This verifies that under unbalanced faults, the proposed protection method is highly discriminative (including HIFs) and is not affected by active power variation of the loads in the microgrid.

Regarding the power factor variation (cases 4 and 5), only a very minor impact on the FDI can be observed in Fig. 10, for both balanced and unbalanced faults.

4.3. Impact of Synchronous Generator (SG)

Considering that a microgrid may contain a Synchronous Generator (SG) in the mix, this section evaluates the potential impact of such SG on the proposed method and evaluates the maximum acceptable SG capacity in the microgrid from the correct protection operation standpoint. In this test, VSC_1 is replaced by an SG with varying capacity. The load power distribution is the same as in case 1 (Table 4).

As in the previous section, the impact is assessed by monitoring the values of FDI under a variety of scenarios with increasing fault resistance. The results are presented in Fig. 11. The fault is assumed to be on line 3 with measured points of bus 3 RHS (inside SFP) and bus 4 LHS (outside SFP) chosen for analysis. Due to its typically low internal impedance, the SG can draw a large proportion of the current from the active injection point, thus influencing the detection capability of the scheme. The convergence value C is also decreased with the increase of SG capacity, making HIF protection less effective especially for balanced faults with resistances above 4Ω. Under unbalanced faults, although the convergence value is lower as a result of SG connection and the discrimination margin is narrower, the threshold setting of $0.2C$ still allows for clear distinction between the conditions of inside and outside SFP, as long as the fault can be initially detected. Therefore, it can be concluded that the proposed method can operate in the presence of SG effectively with the performance being only affected during high impedance balance faults above 4Ω. The result validates that the correct

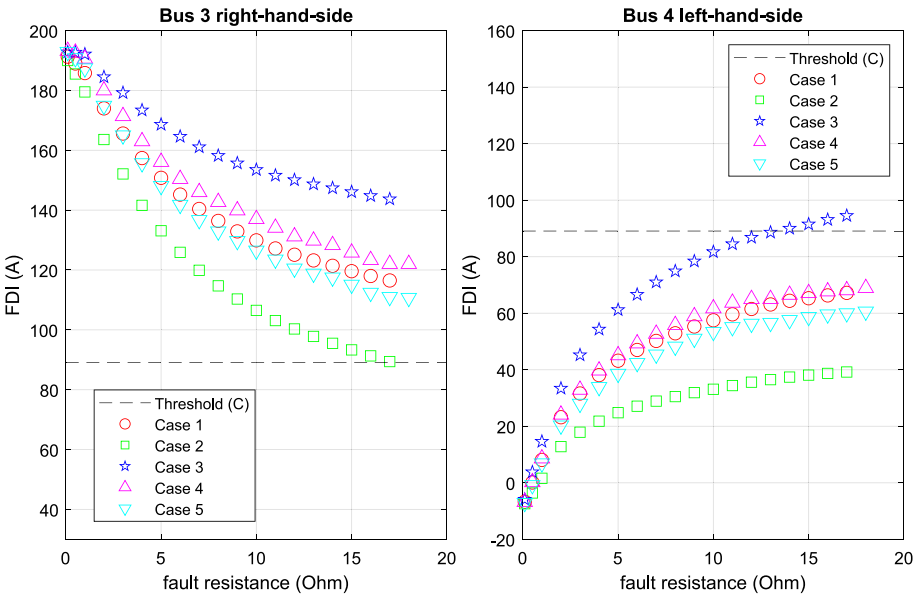

(a) Under balanced faults

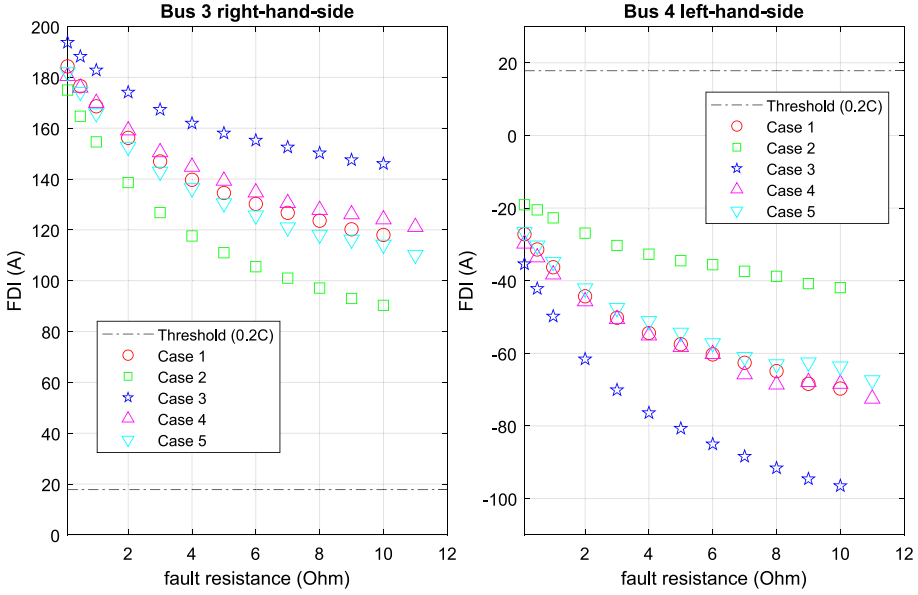

(b) Under unbalanced faults (BC-E)

Fig. 10. Impact of load power distribution on FDI (Fault in line 3).

fault direction identification can be maintained under unbalanced faults with SG capacities up to 30 MW, i.e., 1.2 times the total load power of the test microgrid, which should cover most practical situations of islanded microgrids.

4.4. *Comparative study of the proposed method*

The comparative study of the proposed scheme with other microgrid protection methods has been demonstrated in Table 6. It can be observed that the advantages of proposed method are cost-effective, flexible to implement and reliable under the load disturbance, since only one active DG is required in this scheme without any location limitation or communication requirement and the protection setting strategy has ensured a large sensitivity margin. Although the maximum detectable fault resistance of the proposed method could be lower than few differential protection and artificial intelligence-based protection methods as in [10] and [22], the excellent performance of proposed method under HIF is still notable among existing protection methods for microgrids. Furthermore, the scheme includes inherent backup functionality through time graded tripping logic, which is not provided by many other protection methods.

There are two limitations for the proposed scheme. Firstly, the voltage component-based fault detection method might work incorrectly under the severe single-phase load disturbance when a huge negative sequence voltage/current is generated, besides, the highly resistive fault becomes hard to be observed when it comes to the large-scale network, thus improving the fault detection method can be the further work especially in the large system, like using signal processing-based or AI-based methods to detect the fault. Secondly, the time delay due to the active current injection progress, i.e., the waiting time of current dynamics at pre-injection and current generation stages as shown in Fig. 4, makes the proposed method own a longer operating time, which can be a potential weakness when compared with communication-based methods such as differential protection, traveling wave-based protection and so on. However, the scheme is more economical in practical microgrid applications without communication

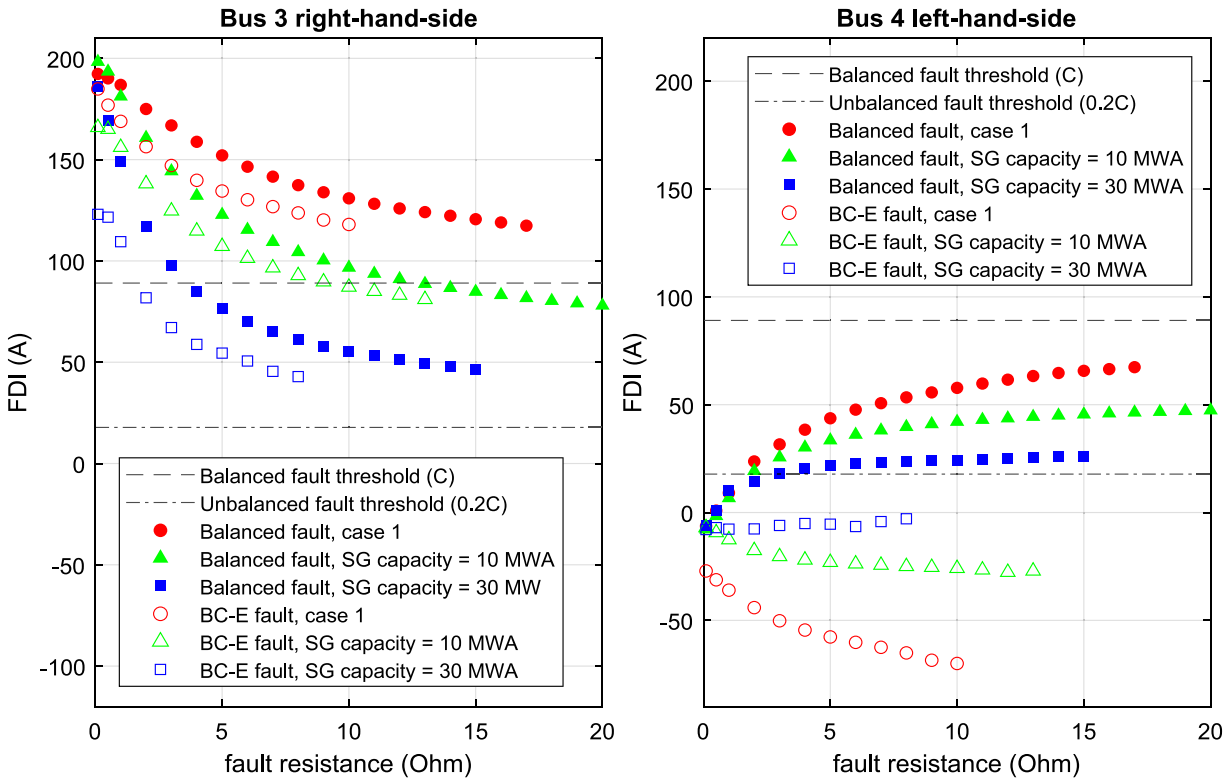

Fig. 11. Impact of SG capacity on FDI (Fault in line 3).

Table 6
Comparison of the proposed scheme with other protection methods.

Methods for comparison	Advantages of proposed method	Disadvantages of proposed method
Overcurrent protection [21]	• Convenient power flow analysis by using the NPS component-based circuit. • Less sensitive to loading condition.	N/A
Differential protection [4,22]	Without communication, cost-effective	Slow operation Weak HIF detection capability
Traveling wave-based protection [5,6]	Without communication, cost-effective	Slow operation
Adaptive protection [7]	• Simple in operation • Less calculation algorithm	Slow operation
Artificial intelligence-based protection [10]	Simple in operation	Weak HIF detection capability
Harmonic injection-based active protection [15,16]	• Flexible to use with only one active DG, without the limitation of installation location. • More compatible with power system	N/A
Harmonics contents-based protection [12]	Large sensitivity margin	Slow operation

requirement, while still preserving excellent discrimination. Thereby, the proposed method can be particularly suited to smaller scale microgrids where overall cost can become a barrier.

4.5. Implementation in a large network

To validate the operation of the proposed method in a larger network, the scheme is implemented in the modified IEEE 13-bus system with additional DGs as shown in Fig. 12. The network is operated in a balanced loading condition and the system parameters are included in Table 7. The VSC_6 is voltage-controlled and the remaining VSCs at other buses are current-controlled. The VSC_8 is the dedicated active DG for NSCI during the fault. The FDIs at the measured point of bus 3 (on the side of line 9) are used for analysis when balanced and unbalanced faults occur on line 3, 9 and 11, and the test results are summarized in Fig. 13 with increasing fault resistance values. When the measured point is inside SFP (Fault in line 3), the FDIs are always above the threshold (marked in red), providing the fault remains within the high impedance detection limit. When the measured point is outside SFP (Fault in line 9 & 11), the FDIs are always below the C for balanced faults, and lower than $0.2C$ under unbalanced faults. Therefore, the proposed protection strategy is shown to work effectively in a larger network such as the IEEE 13-bus system.

In the large-scale network with complicated topology and high number of buses, the NSCI method may fail to detect the fault, and therefore, may not trigger the dedicated active DG. Moreover, the capacity of one dedicated VSC might not be sufficient to ensure the flow of injected current into the entire system, thus the relays located at the far end of some branches may not be able to capture the current increment.

However, with careful design, it should be possible to implement the proposed method in a complex network, using one of the two suggested approaches:

- Splitting the network into a few zones and including the active DG for injection in each zone. In this way, the fault current becomes more obvious in the small zone and the fault can be detected by the relay at injection bus (active DG can be triggered).
- In the cases where discrimination is not required for all individual lines, a possible solution is to consider several buses (e.g. at the remote part of the microgrid) as a group, dedicating one selected relay to protect this group of buses instead of protecting each line. In this way, the grouped buses/loads can draw sufficient amount of injected current from active DG and the scheme can still operate effectively.

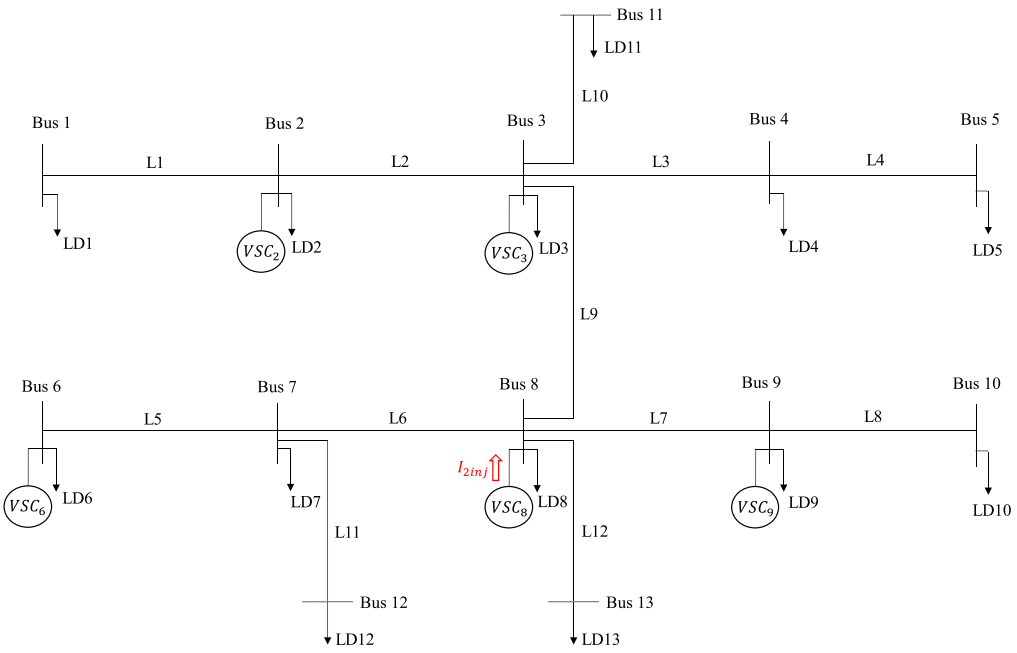

Fig. 12. Modified IEEE 13-bus system [23].

Table 7
Parameters of the modified IEEE 13-bus system.

Simulation parameters	Value
Nominal voltage	11 kV
Nominal frequency	50 Hz
DG rating	10 MVA for each DG
Filter impedance	0.242 + j2.42 Ω for each DG
DG reference power	9 MW at bus 2; 9 MW at bus 3; 6 MW at bus 8; 8 MW at bus 9
Line impedance	0.1 + j0.1 Ω/km for each line
Line length	1 km for each line
Load power	2.5 MW at bus 1; 4 MW at bus 2; 3 MW at bus 3; 4 MW at bus 4; 3 MW at bus 5; 6 MW at bus 6; 3 MW at bus 7; 4 MW at bus 8; 2.5 MW at bus 9; 3 MW at bus 10; 2 MW at bus 11; 2 MW at bus 12; 1 MW at bus 13;

5. Conclusion

This paper proposes a novel NSCI-based active protection scheme for an islanded microgrid. The theoretical foundations and the principle of operation of the scheme are explained, including fault detection, fault type discrimination, current angle selection indicator measurement, NSCI control algorithm, fault direction indicator measurement, and the time-graded coordination of the relays which facilitates backup. The rationale for the best compromise protection settings is also developed based on the sequence network analysis during the active injection progress. The simulation-based performance evaluation validates the reliable behavior of the proposed method under a variety of influencing factors such as the fault type, faulty section, load power distribution and power factor, as well as potential presence of SG.

The key advantages for the scheme over passive schemes can be summarized as follows:

- The operation of the scheme is determined by the clearly defined active response of a single converter in the microgrid, and therefore, does not depend on the behavior or other inverter connected sources which can vary in design, fault response and dynamic behavior.
- The scheme can be cost effective as only fundamental frequency signals (phasors) are used, and no communication between the relays is required.
- The scheme only requires one dedicated DG to inject current without location constraint. This enhances the flexibility of the proposed method in practical applications.
- The scheme has a strong capability to detect and discriminate during high impedance faults. This is particularly evident during unbalanced faults which form a vast majority of all faults in there-phase systems.
- Due to the use of incremental value measurement and detection, the scheme maintains high performance under changing network loading conditions.
- The scheme can cope with the presence of a synchronous generator and other inverter connected sources.
- The time-graded coordination of the relays facilitates protection backup.
- The active injection method is implemented using a relatively minor modification to the existing current control of the converter, which enables one of the DGs to operate temporarily as a negative sequence current source with controllable amplitude and phase angle.

The above advantages make the proposed solution a very attractive candidate when it comes to protecting a converter-dominated islanded microgrid. Further validation of the scheme will be performed using Hardware-in-the-loop (HiL) setup in a real-time laboratory environment.

CRediT authorship contribution statement

Zhenkun Yang: Writing – original draft, Visualization, Validation, Software, Resources, Project administration, Methodology, Investigation, Formal analysis, Data curation, Conceptualization. **Adam Dyśko:** Writing – review & editing, Supervision, Software, Project administration, Methodology, Funding acquisition, Formal analysis, Conceptualization. **Agustí Egea-Àlvarez:** Supervision, Software, Methodology.

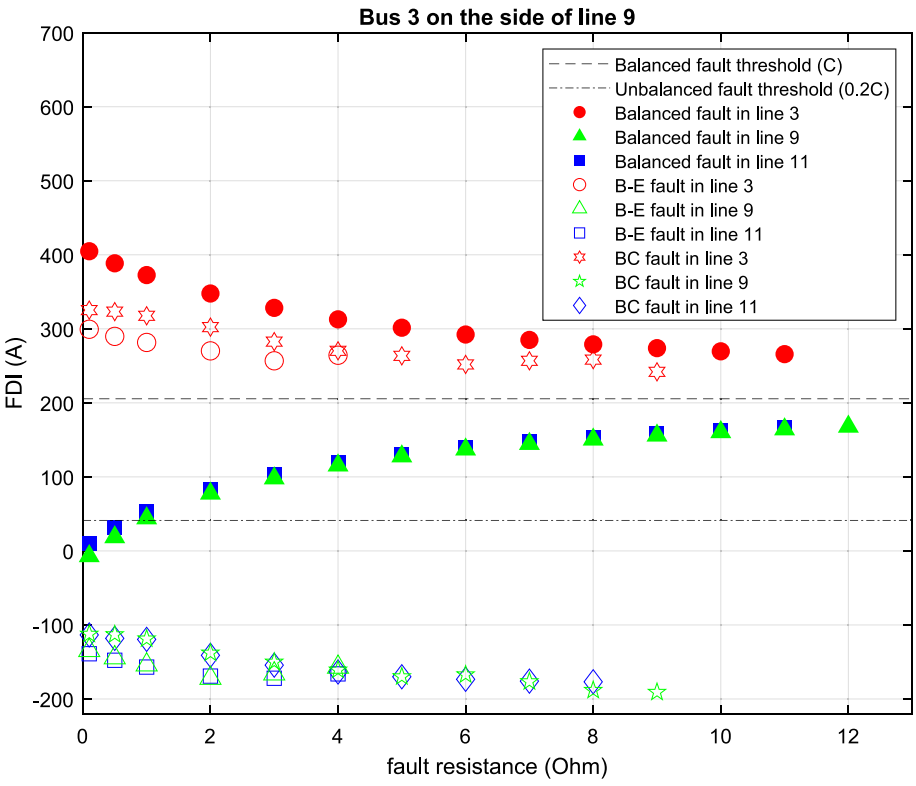

Fig. 13. Implementation in the modified IEEE 13-bus system.

Declaration of competing interest

The authors declare that they have no known competing financial interests or personal relationships that could have appeared to influence the work reported in this paper.

Data availability

No data was used for the research described in the article.

References

[1] Committee on Climate Change, Net Zero Technical Report, pp. 19–292, 2019.
[2] Nadeeb AN, Sequence components based detection and classification of faults in an islanded distribution system with 100% inverter based resources, 2020, 1–42.
[3] Guobin C, Yiqing L, Qifan Y. Impedance differential protection for active distribution network. IEEE Trans Power Deliv 2020;35(1):25–36.
[4] Dewadasa M, Ghosh A, Ledwich G, Protection of microgrids using differential relays. In: 2011 21st Australas. Univ. Power Eng. Conf. AUPEC 2011, 2011, pp. 1–6.
[5] Li X, Dysko A, Burt GM. Traveling wave-based protection scheme for inverter-dominated microgrid using mathematical morphology. IEEE Trans Smart Grid 2014;5(5):2211–8.
[6] Liu D, Dysko A, Hong Q, Tzelepis D, Booth C. Transient wavelet energy based protection scheme for inverter-dominated microgrid. IEEE Trans Smart Grid 2022; 13(4):2533–46.
[7] Bhattarai BP, Bak-Jensen B, Chaudhary S, Pillai JR, An adaptive overcurrent protection in smart distribution grid. In: 2015 IEEE Eindhoven PowerTech, PowerTech 2015, 2015.
[8] Yi H, Hu X, Dongxia Z. Study of adaptive fault current algorithm for microgrid dominated by inverter based distributed generators. In: 2nd Int. Symp Power Electron Distrib Gener Syst PEDG 2010; 2010. p. 852–4.
[9] Coffele F, Booth C, Dyśko A. An adaptive overcurrent protection scheme for distribution networks. IEEE Trans Power Deliv 2015;30(2):561–8.
[10] Sarwar M, Mehmood F, Abid M, Khan AQ, Gul ST, Khan AS. High impedance fault detection and isolation in power distribution networks using support vector machines. J King Saud Univ - Eng Sci 2020;32(8):524–35.
[11] Al-Nasseri H, Redfern MA, O'Gorman R. Protecting micro-grid systems containing solid-state converter generation. In: 2005 Int Conf Futur Power Syst; 2005. p. 1–5.
[12] Al-Nasseri H, Redfern MA. Harmonics content based protection scheme for micro-grids dominated by solid state converters. In: 2008 12th Int Middle East Power Syst Conf MEPCON; 2008. p. 50–6.
[13] Microgrids II, Soleimanisardoo A, Karegar HK, Zeineldin HH, Member S, Differential frequency protection scheme based on off-nominal frequency injections for inverter-based islanded microgrids. In: IEEE Trans. Smart Grid 10(2) 2107-2114, vol. 10, no. 2, pp. 2107–2114, 2019.
[14] Chen Z, Pei X, Yang M, Peng L, Shi P. A novel protection scheme for inverter-interfaced microgrid (IIM) operated in islanded mode. IEEE Trans Power Electron 2018;33(9):7684–97.
[15] Khan MAU, Hong Q, Egea-Àlvarez A, Dyśko A, Booth C. A communication-free active unit protection scheme for inverter dominated islanded microgrids. Int J Electr Power Energy Syst 2022;142(PA):108125.
[16] Saleh K, Allam MA, Mehrizi-Sani A. Protection of inverter-based islanded microgrids via synthetic harmonic current pattern injection. IEEE Trans Power Deliv 2021;36(4):2434–45.
[17] Ghaderi A, Mohammadpour HA, Ginn H. Active fault location in distribution network using time-frequency reflectometry. In: 2015 IEEE Power Energy Conf Illinois, PECI 2015; 2015. p. 1–7.
[18] Telukunta V, Pradhan J, Agrawal A, Singh M, Srivani SG. Protection challenges under bulk penetration of renewable energy resources in power systems: A review. CSEE J Power Energy Syst 2017;3(4):365–79.
[19] Kareem Al-Sachit S, Javad Sanjari M, Nair N-KC, Negative sequence-based schemes for power system protection-review and challenges, 2018.
[20] National Electrical Manufacturers Association, American National Standard Electric Power Systems and Equipment-Voltage Ratings (60 Hertz)-ANSI C84.1: Service Voltage Limits for Systems Greater Than 600 V, 2011.
[21] Khan MAU, Hong Q, Dyśko A, Booth C. Performance analysis of the overcurrent protection for the renewable distributed generation dominated microgrids. 2020 IEEE Region 10 Symposium (TENSYMP), 5-7 June 2020, Dhaka, Bangladesh. 2020.
[22] Farkhani JS, Wang H, Chen Z, Leth Bak C. Differential-based protection scheme to protect active distribution network. International Journal of Electrical Power & Energy Systems. 2017.
[23] Tamp F, Ciufo P. A sensitivity analysis toolkit for the simplification of MV distribution network voltage management. IEEE Trans Smart Grid 2014;5(2): 559–68.